The high activity of mesoporous Ga-SiO_2 catalysts in the upgrading of glycerol to solketal explained by in-depth characterization

Alvise Vivian,[a] Loraine Soumoy,[a] Luca Fusaro,[a] Pierre Louette,[b] Alexandre Felten,[b] Sonia Fiorilli,[c] Damien P. Debecker,[d],* and Carmela Aprile[a],*

[a] Unit of Nanomaterials Chemistry (CNANO), Department of Chemistry, University of Namur, 5000 Namur, Belgium

[b] SIAM, Department of Physics, University of Namur, 5000 Namur, Belgium

[c] Department of Applied Science and Technology, Politecnico di Torino, 10129 Torino, Italy

[d] Institute of Condensed Matter and Nanosciences – Université catholique de Louvain (UCLouvain), 1348 Louvain-la-Neuve, Belgium

Abstract: Mesoporous Ga-silicates were prepared using a sustainable and continuous aerosol synthesis procedure. The novel solids showed record activity in the synthesis of solketal from glycerol and acetone. Three different Si/Ga ratios of 34, 74 and 148 were investigated and all materials displayed favorable features for catalytic applications such as high surface area and calibrated mesoporosity. An in-depth characterization allowed to elucidate the remarkable catalytic performance. The insertion of Ga predominantly as single site in tetrahedral coordination in the silica framework was highlighted by X-ray photoelectron spectroscopy (XPS), using the Auger parameter of Ga in a Wagner plot representation. The speciation of Ga was further clarified using solid state ^{71}Ga NMR spectroscopy, confirming the formation of mainly isolated Ga species. Consistently, the aerosol-made Ga-silicates displayed outstanding turnover frequencies (up to 677 h^{-1}) and selectivity, markedly outcompeting other reference metallosilicate catalysts reported in literature. Moreover, the most active catalyst was successfully reused in multiple catalytic cycles thus proving its stability under the selected reaction conditions.

Keywords: glycerol valorization, ^{71}Ga NMR; XPS Wagner plot; mesoporous materials; aerosol-assisted sol-gel

1. Introduction

Mesoporous metallosilicate materials are an important class of structured solids possessing high specific surface area, large pore volume and rich surface chemistry. A large number of applications have been proposed in the fields of adsorption, pollutant remediation, sensors, drug delivery and catalysis [1, 2]. The importance of silica-based materials is further enhanced by the possible functionalization of the surface as well as by the selective isomorphic substitution of silicon with different elements. Both approaches constitute a key pillar in the preparation of innovative heterogeneous catalysts. For instance, the insertion as single-site of trivalent cations such as Ga^{3+} is associated with the generation of Brønsted and Lewis acid sites, useful for a wide range of catalytic reactions [3-5]. The introduction of gallium within the silica architecture resulted in improved catalytic performances in the aromatization of olefins and paraffins [6-8]. Mesoporous gallium silicates have also been exploited for a series of sustainable chemical processes including the synthesis of alkyl lactates and other valuable chemicals from glycerol and its derivatives [9, 10]. In particular, it has been already reported that Ga-MCM-41 nanoparticles are one of the most efficient heterogeneous catalysts in the conversion of glycerol into solketal [9].

Recently, the aerosol-assisted sol-gel process emerged as an effective method to produce structured mesoporous silica-based catalysts presenting a metal inserted as single site in the framework [11]. The method implies the atomization of a solution containing molecular precursors which undergo inorganic polycondensation during the rapid drying of the aerosol droplets. By applying this process in the presence of a sacrificial pore-generating agent (e.g. amphiphilic surfactant which self-assemble into micelles under the effect of solvent evaporation) it is possible to design mesostructured particles with a precise control on the texture [12-15]. The advantages of this process combine a reduced waste generation, a limited number of steps, and low environmental impact [16]. In addition, the process for the preparation of catalysts can be easily scaled up and can be run in a continuous mode, making it attractive from an industrial perspective [11, 17]. Aerosol processes have already found application in the production of several metallosilicates displaying excellent catalytic performance in numerous chemical reactions. A few examples are the production of SiAl oxides for hydrocarbon cracking, SiW and SiMoAl oxides for the metathesis of olefin, SiTi

oxides for selective oxidation and recently the synthesis of surface functionalized metallosilicate catalysts for the synthesis of lactates [12, 18-24].

In the synthesis of metallosilicate catalysts, a central pillar is represented by the investigation of the coordination number/geometry of the metal centers inserted as single site within the silica matrix. Describing and quantifying the different species is of fundamental importance since it is strongly correlated with the catalytic performance. In the case of gallium silicates, an in-depth characterization of the coordination environment of gallium is rarely reported in literature. The low gallium concentration in the solids, frequently surrounded by an amorphous environment, makes the characterization of these materials very challenging.

Solid state NMR spectroscopy of $^{71/69}$Ga and X-ray photoelectron spectroscopy (XPS) are two powerful characterization techniques that can be embraced to elucidate the nature of Ga environment. The possibility to use solid state $^{69/71}$Ga NMR has been reported in few studies involving crystalline zeolitic gallosilicates and Ga-MCM-41 solids with the aim of both detecting and distinguishing the contribution related to tetrahedrally and octahedrally coordinated gallium atoms in these structures [25-28]. However, solid state gallium NMR remains challenging due to the quadrupolar nature of both isotopes that are affected by quadrupolar broadening. Despite this, we were able to measure even higher Si/Ga ratios compared to the previously reported studies, working under high magnetic field and using high magic angle spinning (MAS) frequencies to reduce the chemical shift anisotropy effects [29]. For the same purpose, XPS and chemical speciation plots have been extensively employed as useful tools to determine the degree of metal insertion in silica-based solids. As an example, the use of XPS via the Auger parameter in a Wagner plot representation, allowed to separate contributions related to intra- and extra-structural zinc species within the same Zn-MCM-41 sample [30]. In spite of this, only few such XPS studies have considered gallium and in particular only two examples describing the use of a Wagner plot for gallium compounds have been reported in the literature until now [31, 32].

In the present work, a deep structural investigation of Ga-silicates prepared for the first time using the aerosol assisted process provides strong evidences of the relation between the nature of Ga species and their catalytic activity. The insertion of gallium as single site in the silica structure was demonstrated via solid state ^{71}Ga MAS NMR and XPS using the Auger parameter. These materials exhibited high performance in the acetalization of glycerol with acetone to produce solketal, outcompeting other reference catalysts reported in literature. This reaction is of particular relevance in the context of sustainable production of useful bio-based chemicals [33].

2. Experimental

2.1 Characterization

Transmission electron microscopy (TEM) micrographs were collected on a Philips Tecnai 10 microscope using an acceleration voltage of 80 kV. The amount of metal (gallium) in the catalysts was obtained by inductively coupled plasma optical emission spectroscopy (Optima 8000 ICP-OES Spectrometer). The samples were prepared digesting 10 mg of the material in a mixture of 100 µL of aqua regia and 600 µL of HF 48%. Nitrogen adsorption-desorption isotherms were acquired at 77 K with a Micromeritics Tristar 3000 volumetric adsorption analyzer. The samples were outgassed under reduce pressure at 150°C overnight before the analysis. To calculate the specific surface area, the Brunauer–Emmet–Teller (BET) method was applied to the nitrogen adsorption-desorption isotherms in the 0.05-0.20 relative pressure range. The mean pore diameter was determined from the adsorption branches of the isotherm using the Barrett-Joyner-Halenda (BJH) method. The total pore volume (V_t) was derived from the quantity adsorbed at a relative pressure of 0.99.

^{71}Ga solid state NMR magic angle spinning (MAS) spectra were recorded at room temperature on a Bruker Avance-500 spectrometer operating at 11.7 T using a 2.5 mm Bruker CP-MAS probe. The solids were prepared in a 2.5 mm zirconia rotor and analyzed with a spinning frequency of 25000 Hz. The spectra were recorded using an Hahn echo sequence and the following acquisition parameters: a relaxation time of 0.3 s, an excitation of 2.6 µs (90°) and an acquisition time of 16 ms. Data processing includes the multiplication of the FID (Free Induction Decay) by a line broadening factor of 1000 Hz, zero-filling, Fourier transformation and phase and baseline corrections. Fourier transformation from the echo maximum ensured a flat baseline with only zero-order phase correction. The chemical shift scale was calibrated at room temperature using $Ga(NO_3)_3$ as the reference compound (0.0 ppm).

X-ray photoelectron spectroscopy characterizations were carried out on a ThermoFisher ESCALAB 250Xi spectrometer, using a monochromatic Al Kα X-ray source (1486.6 eV) and a hemispherical deflector analyzer (SDA) working at constant pass energy

(CAE). The diameter of the X-ray spot was set to 300 µm. The base pressure of the analyzer chamber was amounted to $2 \cdot 10^{-8}$ Pa. A flood gun, using electrons and Ar ions, was used to compensate for charges induced by photoemission. Survey spectra were recorded with a pass energy of 150 eV that was decreased to 25 eV for high-resolution spectra. Chemical components on photoemission spectra as well as Auger signals were fitted with Gaussian-Lorentzian lineshape. The Gaussian-Lorentzian (L/G) ratio, FullWidth at Half Maximum (FWHM), kinetic energy and intensity (peak area) were adjusted during the procedure.

Brønsted and Lewis acidity of the sample Ga-74 were investigated by Fourier Transform Infrared Spectroscopy (FT-IR) coupled with ammonia adsorption. FT-IR measurements were carried out in transmission mode using a Bruker Tensor 27 spectrometer equipped with a liquid nitrogen-cooled mercury–cadmium–telluride (MCT) detector, working at a 2 cm^{-1} resolution. A pre-treatment was carried out in an IR cell equipped with KBr windows using a standard vacuum frame. Before adsorption of ammonia at room temperature, the sample was compressed into self-standing wafers and outgassed 1h at 400 °C.

Adsorption of ammonia was studied in the pressure range 0.01–20.0 mbar: the reversible fraction of the adsorbed ammonia was then evacuated at room temperature by prolonged outgassing.

In temperature-programmed desorption of ammonia (NH_3-TPD) analyses, 50 mg of sample was introduced in a quartz reactor on a Hiden Analytical Catlab-PCS instrument. Prior to the analysis, the sample was treated in a dry air flow (30 $mLmin^{-1}$) at 550 °C for 2 hours. Consequently, it was cooled down to 50 °C and then exposed to a gas mixture of 5% NH_3 in He (10 $mLmin^{-1}$) and Ar (20 $mLmin^{-1}$) for 45 min. Physisorbed NH_3 was evacuated by purging with Ar (30 $mLmin^{-1}$) 90 min at 50 °C. The TPD analysis was performed by heating the sample from 50 to 650 °C with ramping rate of 5 °$Cmin^{-1}$. Desorbed NH_3 was detected using a mass spectrometer (QGA model).

2.2 Synthesis of Ga-silicates by aerosol-assisted sol-gel

Solution A was prepared by pre-hydrolysis of TEOS (97%; $5.5 \cdot 10^{-3}$ mol; 12 g, TCI) in HCl 0.01 M (0.6 mol; 20 g; pH 2). Solution B was prepared by solvating the structuring agents ($0.68 \cdot 10^{-3}$ mol; 3.9 g Pluronic P123, Sigma Aldrich) in absolute ethanol (45 g) and HCl 0.01 M (0.22 mol; 8 g; pH 2). Solutions A and B were stirred (300 rpm) at room temperature for 40 minutes and 15 hours, respectively. The gallium precursor ($Ga(NO_3)_3 \cdot xH_2O$, ROTH) was then added to solution A at the desired Si/Ga molar ratio. When the metal precursor was dissolved, solution B was added to solution A and the mixture was stirred for 30 minutes (300 rpm). The sol was then atomized (2 bar) using a TSI 6-Jet 9306A atomizer, resulting in aerosol droplets that were dried by passing through a quartz tube heated to 350°C. The obtained powder was collected on a cellulose filter (0.45 µm), dried overnight at 80°C and then calcined in air at 550°C for 5 hours (ramp: 1°C/min).

In the case of pristine SiO_2, the same synthesis procedure was followed by omitting the addition of the gallium precursor.

2.3 Synthesis of Ga/SiO_2 by dry impregnation

A gallium nitrate solution was prepared by adding 500 µL of 0.02 M HCl and then 1 mL of absolute ethanol to $Ga(NO_3)_3 \cdot xH_2O$ (0.025 g ; Si/Ga = 37). In a 10 mL beaker, 150 mg of a pure mesoporous silica prepared by the aerosol process (see above) was impregnated, drop by drop, with the gallium nitrate solution. The catalyst was then dried in an oven at 65°C for two hours, and then calcined in air at 550°C for 5 hours. This catalyst is denoted “Ga-impregnated”.

2.4 Catalytic tests

Acetalyzation of glycerol with acetone: in a round bottom flask, 10 mg of the selected catalyst was added in a mixture containing glycerol (99%, 0.01 mol, 0.92 g) and acetone (0.04 mol, 2.32 g). The reaction blend was then vigorously stirred (800 rpm) at 50°C during a selected time. At the end of the reaction, absolute ethanol (3 mL) was added to the reaction media. The catalyst was then isolated by centrifugation (4500 rpm, 10 min) and the supernatant was analyzed by ^{1}H-NMR with DMSO as deuterated solvent.

Leaching tests: in a round bottom flask, 25 mg of the selected catalyst was added in a mixture containing glycerol (99%, 0.01 mol, 0.92 g), absolute ethanol (0.70 mL, 0.55 g) and acetone (0.04 mol, 2.32 g). The reaction blend was then vigorously stirred (800 rpm) at 50°C during 1 h. After this time, the catalyst was isolated by hot filtration (~ 50°C). The filtrate was then centrifuged (4500 rpm, 5 min) and 500 µL of the supernatant was analyzed by ^{1}H-NMR with DMSO as deuterated solvent. The filtrate was kept at 50 °C for another 5 h under 800 rpm stirring. Another NMR analysis of the reaction mixture was then performed.

Recycling tests: in a round bottom flask, 50 mg of Ga-74 was added in a mixture containing glycerol (99%, 0.017 mol, 1.56 g) and acetone (0.068 mol, 3.95 g). The reaction blend was then vigorously stirred (800 rpm) at 50°C during 1 h. At the end of the

reaction, absolute ethanol (3 mL) was added to the reaction media. The catalyst was then recovered by centrifugation (4500 rpm, 10 min) and the supernatant was analyzed by ^{1}H-NMR with DMSO as deuterated solvent. The catalyst was washed three times with acetonitrile and calcined in air at 450 °C for 2 h (rate: 2 °C min^{-1}) and then tested in the same reaction conditions. The subsequent catalytic tests were carried out by repeating this procedure and by adapting the amount of reactants as a function of the mass of recovered catalyst.

3. Results and Discussion

3.1 Physicochemical properties and Ga coordination environment of Ga-silicates catalysts

The aerosol-assisted sol-gel process was employed to synthesize three different Ga-silicates, bearing respectively a nominal silicon to gallium ratio of 37 (Ga-37), 74 (Ga-74) and 148 (Ga-148). All the materials were characterized using several techniques, inter alia, transmission electron microscopy (TEM), X-ray photoelectron spectroscopy, ^{71}Ga solid-state NMR spectroscopy, N_2 physisorption, and ICP-OES. The characterization of pristine SiO_2 solids, synthesized under the same conditions, is reported in the supporting information (Figure S1, Table S1). The differences between the SiO_2 solids and the gallium containing materials in terms of structural and textural properties could be ascribed to the different composition of the synthesis mixture.

All the Ga-silicate solids consist of spherical particles originating from the fast drying of the atomized aerosol droplets (Figure 1). The thermal removal of P123, used as templating agent, allows obtaining well visible “wormlike” mesopores of 6-7 nm in the core together with lamellar domains in the external part of the particles (Figure 1). The particle size distributions of Ga-37, Ga-74 and Ga-148 were estimated via TEM measurements (Figure S2). The quite broad particle size distribution is centered around 100 nm for all Ga-silicates.

The silicon environment of the solids was probed via ^{29}Si DE-MAS NMR (Magic-Angle-Spinning direct excitation) experiments. The spectra (Figure S3) of all materials show a broad signal which can be considered as a combination of ^{4}Q [(SiO_4)Si], ^{3}Q

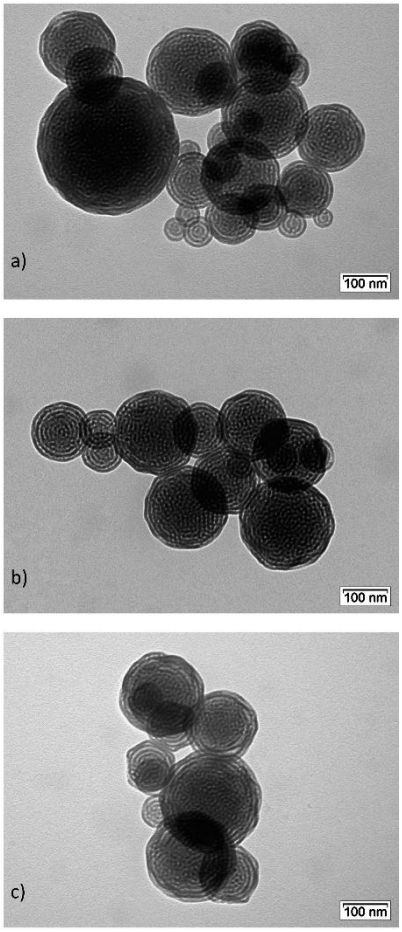

Figure 1. TEM micrographs of Ga-37 (a), Ga-74 (b) and Ga-148 (c) calcined at 550 °C

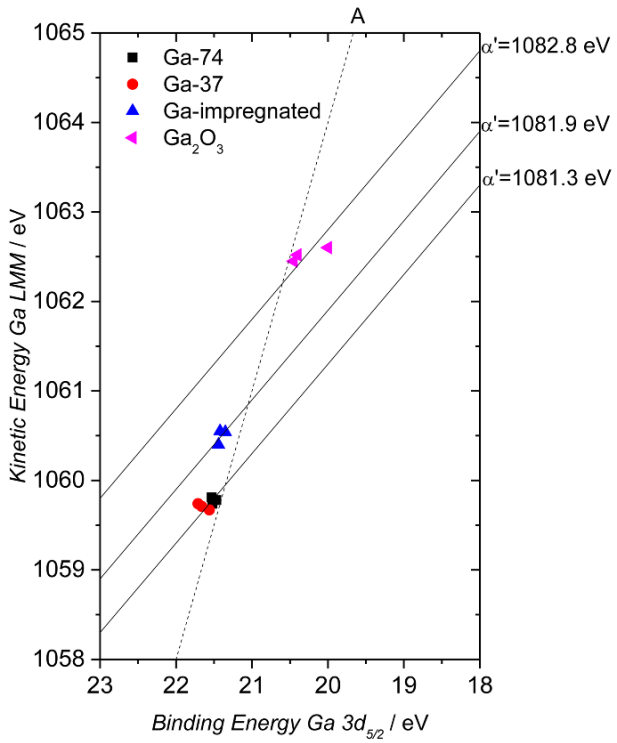

Figure 2. Wagner plot (Ga LMM Auger vs. XPS Ga3d5/2) of Ga-74, Ga-37, Ga-impregnated and gallium oxide

[$(SiO_3)SiOH$] and ^2Q [$(SiO_2)Si(OH)_2$] contributions at around -110 ppm, -102 ppm and -92 ppm, respectively. These signals can be attributed to the presence of an amorphous silica matrix.

The Ga loading was quantified by inductively coupled plasma optical emission spectroscopy (ICP-OES) and the resulting Si/Ga ratios for all the materials were in good agreement with the nominal composition (Table 1). An in-depth characterization to assess the coordination environment of the Ga metal centers present in the silica matrix is of fundamental importance. In this work, the chemical environment of gallium for all the synthesized solids was elucidated using both X-ray photoelectron spectroscopy (XPS) and solid-state ^{71}Ga NMR.

For XPS measurements, hydrated gallium oxide (Ga_2O_3) was chosen as the reference compound and an additional material called "Ga-impregnated" was synthesized taking inspiration from Liu et al [34] to obtain extra-framework gallium species. This material was synthesized by impregnating a pure silica material prepared by the aerosol method with a gallium nitrate solution to obtain a theoretical Si/Ga ratio of 37 (see experimental section). For Ga-148, the Ga signal could not be distinguished from the noise, due a low Ga loading.

As expected, the XPS analysis of standard gallium levels 2p and 3d in Ga-37, Ga-74 and Ga_2O_3 solids did not allow to differentiate significantly the energy contributions associated with the different Ga species (see Figure S4). In the literature, only few studies address the determination of the chemical state of gallium by XPS [31, 32]. The standard use of only chemical shifts of binding energies can be in some cases limiting and for this reason, to better discriminate different energy contributions the use of the Auger parameters is worth to be considered. The graphical representation of the most intense photoelectron line binding energies (abscissa) versus the kinetic energy position of the sharpest Auger line (ordinate) is known as a Wagner plot.

The Auger parameter is the intercept of the linear relationship in equation (1):

$$E_K = \alpha' - E_B \qquad (1)$$

where E_K is the kinetic energy of the Auger electron, α' the modified Auger parameter and E_B is the binding energy of $Ga3d_{5/2}$. This relation can be represented in a Wagner plot on straight lines with slope 1. Moreover, it is possible to show that the relation between E_K and E_B in a Wagner plot can be expressed by the equation (2) [35, 36]:

$$E_K = [const + 2(V_M + kQ)] - 3E_B \qquad (2)$$

$$I = [const + 2(V_M + kQ)] \qquad (3)$$

The value [const + 2(V_M + kQ)] is related to the initial state of the ionized atom, where V_M is the local Madelung potential, Q is the ground-state valence charge and k is the change in core potential resulting from the removal of a valence electron [36]. Equation

(2) shows that compounds with similar initial state effects will appear in a Wagner plot on a straight line with slope 3. Initial state effects can be seen as shifts in the orbital energies of an atom before it is subjected to X-ray irradiation. These effects are generally considered to represent the "chemical shift" as a result of ground state electronic structure and are a function of the valence structure of the core atom. These shifts are related to the electronic states and structural parameters of the bonded atoms.

The Auger parameter and the Wagner plot representation has been used for multiple elements to study the dependence of the local electronic structure on the atomic environments. An example is represented by the study conducted by Bourque et al.[31], where a Wagner plot was used as a tool to differentiate the chemical state of gallium in gallium-cryptand complexes. In addition, Collard et al. [30] showed that it was possible to distinguish, using the Wagner plot, contributions related to zinc as an isomorphic substituent of silicon atoms and extra-structural zinc within the same Zn-MCM-41 sample.

The Wagner plot presented in Figure 2 shows the graphical representation of the most intense photoelectron line binding energies of $3d_{5/2}$ photoelectrons (x) versus the kinetic energy of the most intense core-core-core Auger line (y) for Ga-37, Ga-74, Ga-impregnated and bulk Ga_2O_3. On the Wagner plot, the modified Auger parameters are represented by the plain lines with a slope of 1 and the initial state effects I is represented by the dashed lines with a slope of 3.

According to the study conducted by Wagner and Bourque et al. on the elemental Auger parameter and chemical state plots [31, 37], compounds present on a line with a slope of 3 usually show similar initial state properties (before the interaction with a photon) of the element inside the compound, while in the case of compounds gathered on a line with a slope of 1 (identical modified Auger parameters) similar final state effects are expected (after the interaction with a photon). In Figure 2, all the studied Ga-containing solids are sitting on the same line with a slope of 3 but on different lines with slopes of 1, which suggest that they present differences that can be explained mostly in terms of final state effects [31, 38]. These differences could be attributed to various characteristics such as the particle size, electronic valence, coordination number or the nature of ligands, although some of these can also produce initial state effects. In the case of gallium in hydrated Ga_2O_3, where the coordination environment of gallium is expected to be mainly octahedral, we observe the highest modified Auger parameter (1082.8 eV). The modified Auger parameter

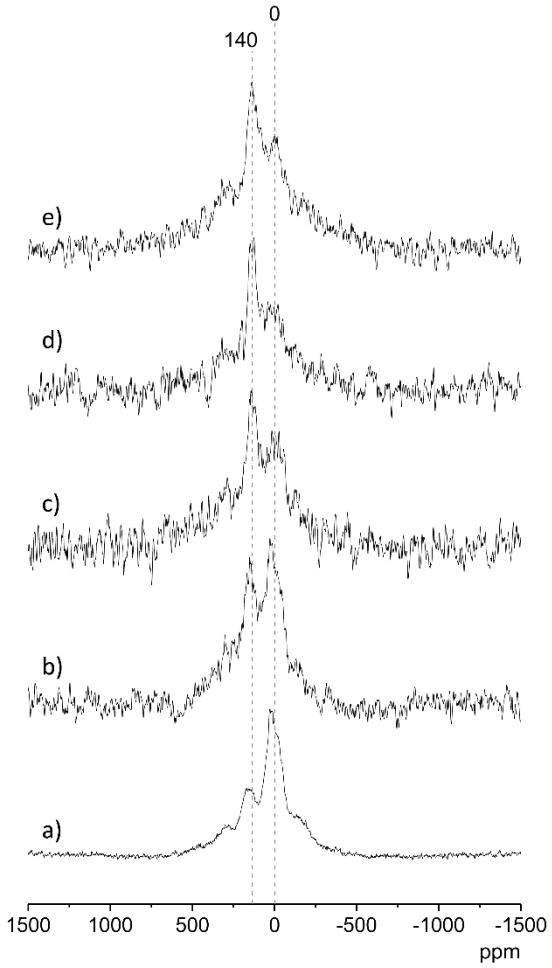

Figure 3. ^{71}Ga solid state MAS NMR spectra of hydrated Ga_2O_3 (a), Ga-impregnated (b), Ga-148 (c), Ga-74 (d) and Ga-37 (e)

of the impregnated Ga-solid is 1081.9 eV and this difference compared to bulk Ga_2O_3 could be attributed to the occurrence of finely dispersed gallium oxide nanoparticles interacting with the silica surface, as reported by Liu et al.[34]. The modified Auger parameter associated with Ga-37 and Ga-74 solids is clearly lower and distinct from those of Ga-impregnated and bulk Ga_2O_3. This lower value of the Auger parameter suggests the presence of tetrahedral Ga inserted in the silica framework. This interpretation is analogous to the work done by Collard et al. [30] on Zn-based materials. It can be noted that the proximity of the energy contributions associated with Ga-37 and Ga-74 solids does not allow to appreciate any difference in the chemical environment of gallium in these two materials.

To further investigate the coordination of gallium, solid state ^{71}Ga NMR spectroscopy was exploited. It is known that solid state NMR spectroscopy is a powerful tool to investigate the coordination number/geometry of metal centers inserted as single sites within the silica matrix. Gallium has two NMR active nuclei, ^{69}Ga and ^{71}Ga, both with a nuclear spin of 3/2 and a natural abundance of 60.1 and 39.8 respectively. It deserves to be mentioned that due to the large second-order quadrupolar broadening, solid state investigation of $^{69/71}$Ga NMR is challenging. Despite to its lower natural abundance, ^{71}Ga was selected in this work due to its smaller quadrupolar moment and slightly higher absolute sensitivity compared to ^{69}Ga. In addition to the intrinsic difficulties of ^{71}Ga, our materials display an unfavorable combination of features for solid state NMR investigations: the presence of an amorphous skeleton together with a low wt% of gallium. In order to obtain precise insights on the coordination of gallium, investigations were performed under magic angle spinning (MAS) at 25 kHz at a high magnetic field (11.7 T).

A sample of β-Ga_2O_3 was measured as standard compound for our NMR investigation. The corresponding spectrum, in agreement with literature data [39], is reported in Figure S5.

Figure 3 shows the MAS NMR spectra of a hydrated sample of gallium oxide, Ga-impregnated, Ga-148, Ga-74 and Ga-37 respectively. The MAS NMR analysis of hydrated gallium oxide shows the presence of a signal centered at 0 ppm with respect to the reference. This signal is attributed to octahedral gallium [29].

The NMR analysis of Ga-37 revealed the presence of a major contribution centered at 140 ppm with respect to the reference. This contribution has already been observed for other gallo-silicates and is ascribed to tetra-coordinated gallium [25, 26, 29]. Nevertheless, the signal shows also a second contribution centered at 0 ppm, which can be associated to the presence of extra-framework gallium. These extra-framework species are expected to have an octahedral environment and to be catalytically inactive [9]. The analysis of Ga-74 evidences a narrower contribution centered at 140 ppm and a contribution at 0 ppm which is proportionally less important, as compared to the case of Ga-37. This indicates the presence of a lower proportion of extra-framework Ga in Ga-74. The ^{71}Ga NMR pattern of Ga-148 was similar to Ga-74, suggesting a similar degree of dispersion in both solids. This finding clearly indicates that among the three synthesized solids a Si/Ga ratio of 74 represents the best compromise between Ga loading and isomorphic substitution and highlights Ga-74 as the most promising catalyst of the series. As expected (and as corroborated by XPS investigation via Wagner plot), the Ga-impregnated solid displays a combination of intra- and extra-framework species which is intermediate between Ga_2O_3 and Ga-37. This behavior can be ascribed to the presence of finely dispersed extra-framework species at the surface, some of them in a distorted tetrahedral environment.

The textural properties and the structure of the solids were examined using N_2-physisorption and powder XRD. An overview of the textural properties of the synthesized Ga-silicates is reported in Table 1. All solids prepared by aerosol had similar texture with a specific surface area around 350 $m^2\ g^{-1}$ and a pore volume around 0.5 $cm^3\ g^{-1}$. They all showed a type-IV isotherm characterized by an evident hysteresis loop that can be classified as a combination of types H1 and H2 (Figure 4, left). The combination of two types of hysteresis may be attributed to the presence of a combination of tubular pores opened at both ends and a more disordered porosity in good accord with TEM observations. The BJH analysis performed on the adsorption branch of the isotherm showed a narrow pore size distribution centered at around 7.5 nm for all the solids.

Table 1. Textural properties and composition of Ga-silicate solids

Material	Surface Area ($m^2\ g^{-1}$)	BJH pore width (nm)	Pore Volume ($cm^3\ g^{-1}$)	d[a] (nm)	a_0[b] (nm)	w_t[c] (nm)	Si/Ga[d]
Ga-37	350	7.5	0.5	8.8	10.2	2.7	38
Ga-74	350	7.0	0.5	8.8	10.2	3.2	79
Ga-148	380	7.7	0.5	8.8	10.2	2.5	160

[a] *d* spacing = $n\lambda/2\sin\theta$, [b] inter-reticular distance $a_0 = 2d/\sqrt{3}$, [c] determined as difference between a_0 and pore width, [d] determined via ICP-OES analysis

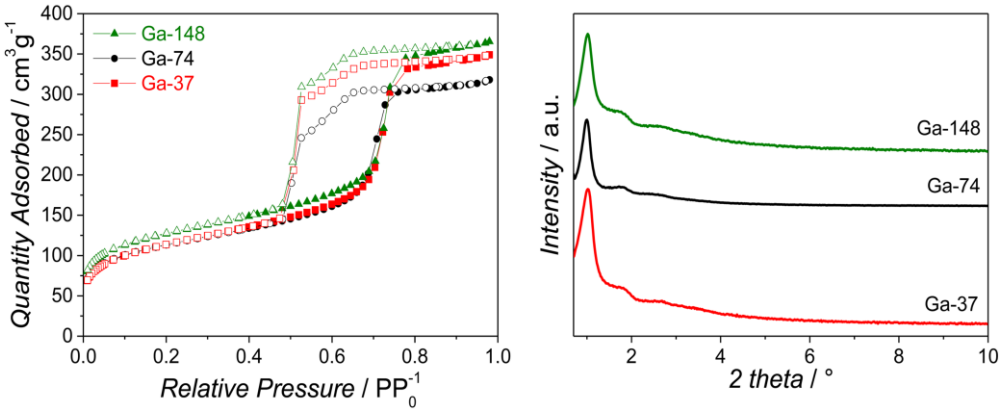

Figure 4. Nitrogen adsorption/desorption isotherms of Ga-silicate solids (left) and small-angle XRD patterns (right)

The low angle powder XRD patterns of Ga-silicates (Figure 4, right) featured an intense first order d_{100} diffraction peak centered at 2θ = 1.0° accounting for the mesostructuration of these solids. A second weaker contribution can be observed and is assigned to the d_{110} reflection. Considering the lattice parameter (a_0) together with the pore diameter determined via N_2 physisorption analysis, the wall thickness of the solids can be calculated. All solids present similar wall thicknesses that lies in the order of 3 nm.

Wide angle XRD patterns (Figure S6) did not show any sharp peak, indicating the amorphous nature of the silica framework and the absence of big clusters of gallium oxide. Nevertheless, this analysis does not allow excluding the presence of small gallium oxide nanoparticles present in the form of extra-framework species as observed through ^{71}Ga NMR measurements in the case of Ga-37 solid.

From TEM, N_2-physisorption and powder XRD investigation, no major differences emerged comparing the morphology and textural properties of the three samples.

Therefore, we can argue that raising the concentration of Ga, in the selected range, does not influence the morphology, texture and structure of the solids. Hence, the eventual catalytic differences can be mainly ascribed to different Ga loading and to different speciation of Ga in the silica structure.

3.2 Acidic properties of Ga-silicates catalysts

The isomorphic substitution of silicon with gallium is known to generate a combination of Lewis and Brønsted acid sites. In order to investigate and compare the acidic properties of Ga-silicates, FT-IR measurements of adsorbed ammonia have been conducted after outgassing the samples at 400°C under dynamic vacuum. The FT-IR difference spectra, (3800-2500 cm^{-1} and 1800-1300 cm^{-1} range) registered upon ammonia adsorption in the same range of equilibrium pressures (0.5-20 mbar), showed as expected very similar spectroscopic features. The FT-IR spectra registered on Ga-74, chosen as representative, are reported in Figure 5.

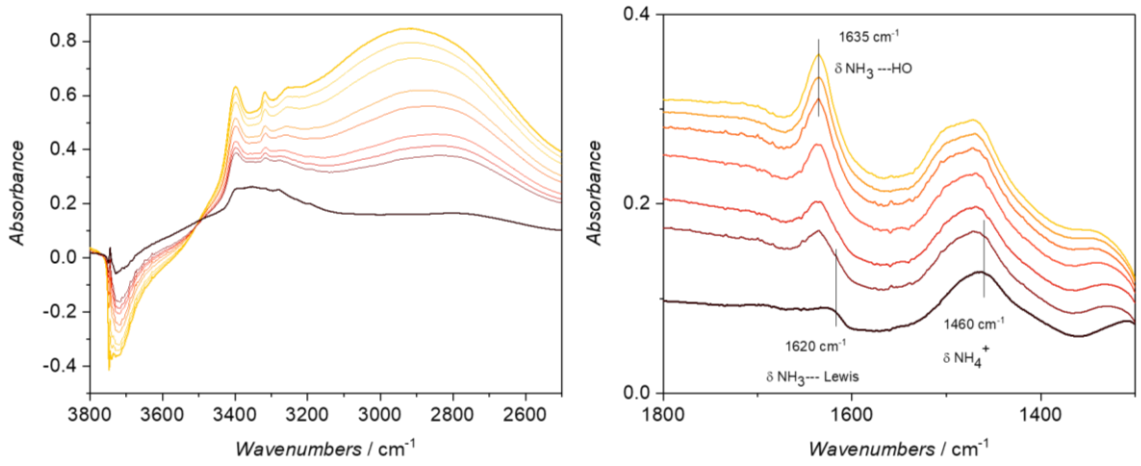

Figure 5. Difference FT-IR spectra of ammonia dosages on Ga-74. The darkest color corresponds to the FT-IR spectrum registered after prolonged outgassing.

The darkest colored curve represents the sample after ammonia dosage and degassing for 30 minutes, useful to understand which fraction of ammonia is reversibly and irreversibly adsorbed.

In the high frequency region of the difference spectra (3800-2000 cm^{-1}), negative absorption bands (associated to species consumed upon dosages) are observed, ascribed to different kinds of hydroxyls interacting with NH_3. A negative band at about 3745 cm^{-1} is due to free silanols and two negative bands at about 3720 and a broad shoulder at 3550 cm^{-1} are related to terminal and H-bonded silanols in hydroxyls chains, respectively [40]. The signals at around 3400 and 3316 cm^{-1} are ascribed to N-H stretching modes, while the broad band is due to the hydroxyl species H-bonded to adsorbed ammonia molecules. In the low region of the spectra, the absorption band at 1635 cm^{-1} is assigned to the bending mode of ammonia molecules H-bonded to hydroxyl groups, whereas the broad signal at around 1460 cm^{-1} is due to the bending mode of NH_4^+ ions generated from proton-transfer reaction on Brønsted acidic groups. This suggests that the incorporation of Ga within the silica framework is able to generate Brønsted sites that are acidic enough to protonate ammonia, at variance with surface hydroxyls of unsubstituted silica materials, which interact with NH_3 via hydrogen-bonding without proton transfer.

Ga-37 and Ga-148 showed very similar spectroscopic features both in the high and in the low frequency region upon ammonia dosages, with difference in the intensity of the band associated to ammonium ion, which as expected was found to be higher for Ga-37 compared to Ga-74 and Ga-148.

In order to better discriminate the acid properties of the three Ga-silicate samples, IR spectra were registered upon a prolonged outgassing at room temperature of dosed ammonia (Figure S7). The observed residual bands are related to species irreversible upon ammonia removal and thus formed on the strongest exposed acidic sites. For fully outgassed samples the signal of NH_4^+ ion decreases upon outgassing (reversible proton transfer) and the different residual intensities for the three samples are in full agreement with the expected concentration of Brønsted sites on the basis of Si/Ga ratios (Ga-37 > Ga-74 > Ga-148).

The absorption band attributed to ammonia on silanols (1635 cm^{-1}) sizably decreased in intensity for the fully outgassed samples (residual pressure < $1 \cdot 10^{-3}$ Pa) and was red-shifted. In addition, after degassing a band at 1620 cm^{-1} became visible, frequency associated to ammonia irreversibly adsorbed on unsaturated Ga^{3+} acting as Lewis sites [40]. This signal appears more intense for Ga-37 (red curve) than for Ga-74 (blue curve) and Ga-148 (green curve), suggesting higher concentration of exposed surface Lewis sites for the higher loading Ga-silicate compared to the other two samples. Furthermore, the intensity of residual signals on Ga-37 indicates that the Brønsted/Lewis ratio on this sample is lower compared to Ga-74 and Ga-148, indicating that by decreasing the Si/Ga ratio the insertion of gallium within the silica framework is less efficient, leading to the formation of larger concentration of extra-framework Ga sites.

From the previous results emerged that two of the three solids (Ga-37 and Ga-74) are highly promising in terms of acidic properties. In order to shed light on the differences between these two solids, the total number of acid sites and their strength was assessed using NH_3-TPD. After adsorption of NH_3 at 50°C and flushing under Ar, 290 $\mu molg^{-1}$ of NH_3 desorbed from Ga-74 in one peak centered at 114°C. This contribution could be assigned mainly to the presence of weak Brønsted acid sites (Figure S8). For the material Ga-37 two desorption peaks are observed, the first at 117°C and a second at 270°C with a total amount of desorbed NH_3 of 360 $\mu molg^{-1}$ (Figure S8). This indicates the existence of a broader Brønsted and Lewis acid-site distribution ranging in strength from weak to moderate. The quantitative data obtained via NH_3-TPD are in good agreement with the findings from FT-IR measurements.

3.3 Catalytic activity in the acetalization of glycerol into solketal

The synthesized mesoporous Ga-silicates present favorable features for their application in heterogeneous catalysis. The targeted reaction selected in this work is represented by the acetalization of glycerol with acetone to produce solketal. Based on literature data, a proposed mechanism catalyzed by Brønsted or Lewis acid catalyst is shown in Figure S9. The associated kinetic model was already extensively expressed in literature by Nanda et al[41].

A kinetic study was performed using Ga-74 as catalyst and the formation of solketal over time was followed in the range of 1h to 16h, reaching a solketal yield of about 55% (Figure 6). Extending the reaction time did not result in a further improvement in the conversion. A similar behavior was already observed in literature [42]. This suggests that the thermodynamic equilibrium is reached and that – at a given reaction temperature – any further improvement in solketal yield could only be obtained by the modifications of reaction conditions which can shift the equilibrium to the formation of the desired product. A well-known procedure

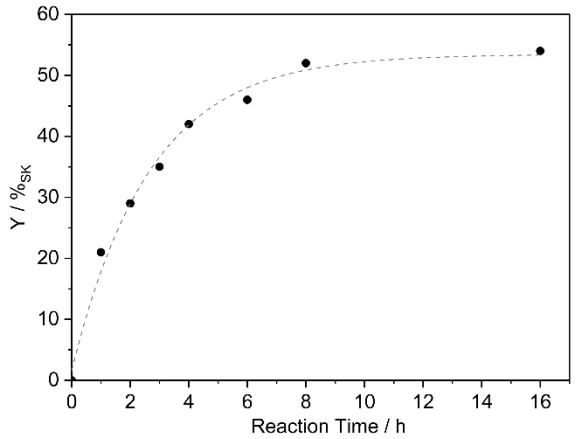

Figure 6. Kinetic study performed using Ga-74 catalyst. Reaction conditions: 10 mg of catalyst, 0.01 mol of glycerol, 0.04 mol of acetone, 50°C.

to beneficially shift the reaction equilibrium is to eliminate water using a Dean-Stark apparatus. Nevertheless, considering the balance between performances and sustainability, an interesting alternative is represented by the design of catalysts having an adequate balance between the hydrophilic-hydrophobic properties of their surface[43]. Another method to shift the equilibrium toward the formation of solketal is to play on the relative amount of reactants. Here, an excess of acetone corresponding to the acetone/glycerol ratio (mol) of 1/4 was used. Indeed, it was already shown that this particular ratio allows to reach the best conversion of glycerol[44].

The kinetic study was used to select an adequate reaction time to compare the catalytic activity of the solids. A reaction time of 2h was selected as the best compromise between an acceptable solketal yield (around 30%) enabling an accurate quantification and a meaningful comparison among the catalysts, but far enough from the equilibrium conversion [45]. Thus, the initial specific activity was approached by considering the activity at 2h, expressed in terms of turnover frequency (TOF, defined as moles of solketal produced per moles of Ga and per hour). To verify the reproducibility of the catalytic tests, all the solids were tested three times under identical reaction conditions. The error measured on the solketal yield was around 2% in absolute value, confirming the good reproducibility of the presented tests.

From a first comparison among Ga-37, 74 and 148 (Table 2) emerged that the catalytic activity does not increase proportionally with gallium loading. In particular, very similar solketal yields were observed when Ga-37 and Ga-74 were tested (compare entries 1 and 2, Table 2) with only a slightly higher yield obtained with Ga-37 that can be ascribed to its higher acidic site concentration, as revealed by the FT-IR and NH_3-TPD characterization.

The decreased turnover frequency (TOF) of the solid Ga-37 compared to Ga-74, based on the number of metal sites, can be explained considering the less efficient insertion of gallium in tetrahedral coordination leading to the formation of a higher quantity of extra-framework gallium species and catalytically less efficient surface exposed Lewis sites [46], as observed via ^{71}Ga MAS NMR and FT-IR. These observations are supported by the evaluation of the TOF of the solid Ga-37 and Ga-74, based on the

Table 2. Catalytic activity of Ga-silicates in the conversion of glycerol to solketal

Entry	Material	Si/Ga	Yield (%)	Sel. (%)	TOF (h^{-1})
1	Ga-37	38	30	85	361
2	Ga-74	79	28	85	677
3	Ga-148	160	10	79	487
4	Ga-impregnated	37	< 2	-	-
5	Ga_2O_3	-	< 2	-	-

Si/Ga ratios determined by ICP-OES analysis; Reaction conditions: 10 mg of catalyst, 0.01 mol of glycerol, 0.04 mol of acetone, 50°C, 2h; TOF = $(n_{solketal}/n_{Ga})$ h^{-1}

number of acid sites (TOF_{acid}) evaluated via NH_3-TPD. The calculated activity, normalized through the number of acid sites is still higher for Ga-74 (TOF_{acid} = 482) compared to Ga-37 (TOF_{acid} = 414).

It is important to underline that extra-framework gallium species are not active in the selected target reaction, as demonstrated here experimentally with bulk gallium oxide and Ga-impregnated which displayed no catalytic activity (see entries 4 and 5, Table 2).

Concerning Ga-148 catalyst, its decreased activity could be attributed to its low Ga loading resulting in the presence of a limited amount of acid sites. Ga-74 afforded the highest TOF. All the materials present a very high selectivity and the only secondary product detected was the six-membered ring compounds (2,2-dimethyl-1,3-dioxan-5-ol).

While we show that the reaction can be run effectively in solvent-less conditions, other works reported in the literature relied on the use of solvents. In order to allow a meaningful comparison of our best catalyst with literature data [9, 47], an additional catalytic test was performed, using t-butanol as solvent. The results gathered in Figure 7 evidence the outstanding catalytic performance of Ga-74 compared not only to previously reported Ga-based catalyst but also to other metal-containing silicates reported in literature (the detailed catalytic results in terms of yield and selectivity are reported in Table S2). This behavior could be due to a favorable combination of features such as high surface area, accessible mesoporosity and insertion of gallium mainly as single site in the silica architecture.

Although the activity of a heterogeneous catalyst is an important parameter, the possibility of using the catalyst in multiple catalytic runs should not be neglected. Recycling tests for the catalyst showing the best activity (Ga-74) are presented in Figure 8. In order to prove the reusability of the catalyst, four consecutive catalytic tests were performed, including reactivation of the catalyst by washing with acetonitrile and calcination at 450°C for two hours (see experimental section). Recycling tests showed that Ga-74 catalyst always maintained an excellent selectivity and an almost stable catalytic activity over four cycles. The absence of leaching of gallium species in solution was verified by ICP-OES analysis on the used catalyst. At the end of the last cycle, the Si/Ga ratio for the reused catalyst remained almost unchanged compared to the fresh one. In addition, the characterization of the catalyst after recycle via N_2 physisorption and ^{71}Ga NMR did not display major differences in comparison to the fresh solid (see Figure S10 and Table S3).

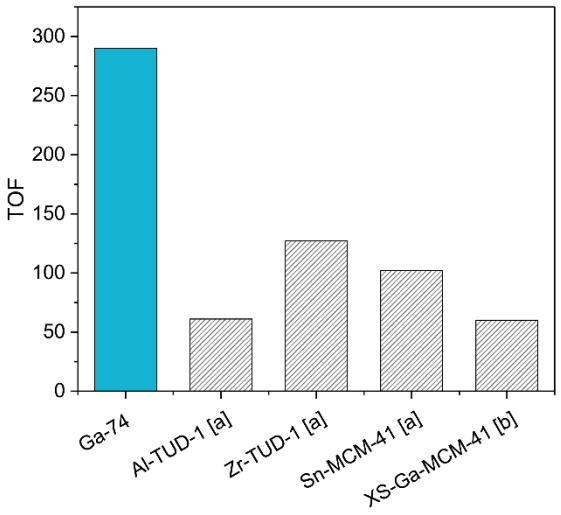

Figure 7. Catalytic activity of Ga-74 in the conversion of glycerol to solketal compared to metal-silicates reported in the literature: [a][47], [b][9]. Reaction conditions: 0.01 mol of glycerol, 1 eq. of acetone, 0.02 mol of t-butanol, 2h and 25 mg of catalyst

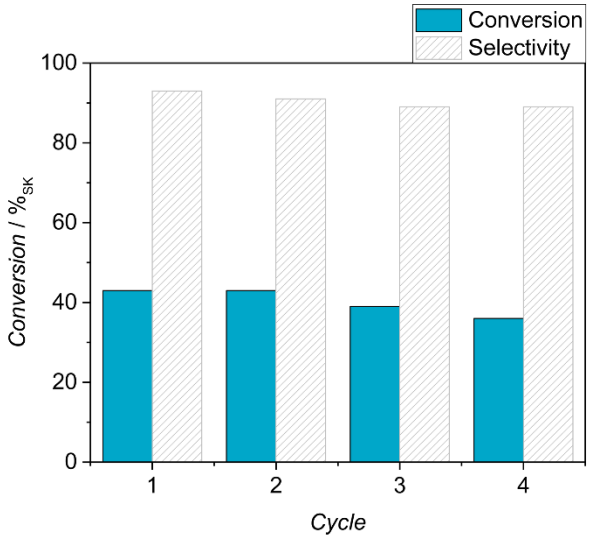

Figure 8. Recycling tests using Ga-74

In order to investigate the stability of the active sites under the selected reaction conditions, a hot filtration test was performed as well (Figure S11, see experimental section for reaction conditions). The solketal yield was quantified after one hour of reaction. The catalyst was then separated from the reaction medium by hot filtration (50°C) and the filtrate was further reacted at 50°C for additional five hours. Figure S11 shows that the solketal yield remained unchanged, indicating the absence of leaching of active sites.

4. Conclusions

The aerosol-assisted sol-gel process was used here as a straightforward synthetic procedure for the synthesis of Ga-silicate catalysts. The solids were characterized via transmission electron microscopy, ICP-OES analysis and N_2 physisorption measurements. The catalysts can be described as spherical gallosilicate particles with well-calibrated mesopores, synthesized with an excellent control on the composition. An advanced XPS analysis using the Wagner plot and ^{71}Ga solid state MAS NMR spectroscopy allowed to deeply investigate the coordination environment of Ga. Importantly, this allowed to evidence the successful isomorphic substitution of Ga in the silica matrix. The presence of Lewis and Brønsted acid sites, fundamental to promote the acetalization of glycerol into solketal, was confirmed via FT-IR of adsorbed ammonia and NH_3-TPD.

The best material, Ga-74, exhibited outstanding catalytic activity in the conversion of glycerol to solketal under solventless conditions. This material clearly outcompetes previously reported Ga-based catalysts. Such high performance was ascribed to the efficient insertion of gallium as single site within the silica framework. Moreover, the catalyst proved to be stable and reusable under the selected reaction conditions in multiple runs. The stability of the catalyst was also supported via full characterization of the solid after the 4th cycle where no major differences were found.

Acknowledgements

Authors acknowledge the 'Communauté française de Belgique' – including the PhD fellowship of A. Vivian – through the ARC programme (15/20-069) and the FNRS through the FNRS-EQP-U.N034.17F for the financial support. L. Soumoy thanks the FNRS for the financial support in the context of her FRIA PhD grant. This research used resources of the "Plateforme Technologique Physico-Chemical Characterization" – PC^2, the SIAM platform (Synthesis, Irradiation & Analysis of Materials) and the MORPH-IM platform (Morphology & Imaging) located at the University of Namur. D.P. Debecker thanks the Francqui Foundation for his "Francqui Research Professor" chair. F. Devred is acknowledged for the technical and logistical support.[9]

References

[1] M.E. Davis, Ordered porous materials for emerging applications, Nature, 417 (2002) 813-821.
[2] Y. Li, J. Shi, Hollow-structured mesoporous materials: chemical synthesis, functionalization and applications, Adv. Mater., 26 (2014) 3176-3205.
[3] B. Jarry, F. Launay, J.P. Nogier, V. Montouillout, L. Gengembre, J.L. Bonardet, Characterisation, acidity and catalytic activity of Ga–SBA-15 materials prepared following different synthesis procedures, Appl. Catal., A, 309 (2006) 177-186.
[4] Z. El Berrichi, B. Louis, J.P. Tessonnier, O. Ersen, L. Cherif, M.J. Ledoux, C. Pham-Huu, One-pot synthesis of Ga-SBA-15: activity comparison with Ga-post-treated SBA-15 catalysts, Appl. Catal., A, 316 (2007) 219-225.
[5] R. Fricke, H. Kosslick, G. Lischke, M. Richter, Incorporation of gallium into zeolites: syntheses, properties and catalytic application, Chem. Rev., 100 (2000) 2303-2406.
[6] G. Giannetto, R. Monque, R. Galiasso, Transformation of LPG into aromatic hydrocarbons and hydrogen over zeolite catalysts, Cat. Rev. - Sci. Eng., 36 (1994) 271-304.
[7] T. Inui, H. Nagata, H. Matsuda, J.B. Kim, Y. Ishihara, Selective synthesis of aromatic hydrocarbons from propylene on gallium-silicate catalysts, Ind. Eng. Chem. Res., 31 (1992) 995-999.
[8] A.P. Singh, K.R. Reddy, Synthesis, characterization, and catalytic activity of gallosilicate analogs of zeolite ZSM-22, Zeolites, 14 (1994) 290-294.
[9] X. Collard, L. Li, W. Lueangchaichaweng, A. Bertrand, C. Aprile, P.P. Pescarmona, Ga-MCM-41 nanoparticles: synthesis and application of versatile heterogeneous catalysts, Catal. Today, 235 (2014) 184-192.
[10] P.Y. Dapsens, B.T. Kusema, C. Mondelli, J. Pérez-Ramírez, Gallium-modified zeolites for the selective conversion of bio-based dihydroxyacetone into C1–C4 alkyl lactates, J. Mol. Catal. A: Chem., 388-389 (2014) 141-147.
[11] D.P. Debecker, S. Le Bras, C. Boissière, A. Chaumonnot, C. Sanchez, Aerosol processing: a wind of innovation in the field of advanced heterogeneous catalysts, Chem. Soc. Rev., 47 (2018) 4112-4155.
[12] A. Sachse, V. Hulea, K.L. Kostov, N. Marcotte, M.Y. Boltoeva, E. Belamie, B. Alonso, Efficient mesoporous silica–titania catalysts from colloidal self-assembly, Chem. Commun., 48 (2012) 10648-10650.
[13] K.Y. Jung, Y.R. Jung, J.-K. Jeon, J.H. Kim, Y.-K. Park, S. Kim, Preparation of mesoporous V_2O_5/TiO_2 via spray pyrolysis and its application to the catalytic conversion of 1, 2-dichlorobenzene, J. Ind. Eng. Chem., 17 (2011) 144-148.
[14] A. Kim, C. Sanchez, B. Haye, C. Boissière, C. Sassoye, D.P. Debecker, Mesoporous TiO_2 support materials for Ru-based CO_2 methanation catalysts, ACS Appl. Nano Mater., 2 (2019) 3220-3230.
[15] F. Colbeau-Justin, C. Boissière, A. Chaumonnot, A. Bonduelle, C. Sanchez, Aerosol route to highly efficient (Co)Mo/SiO_2 mesoporous catalysts, Adv. Funct. Mater., 24 (2014) 233-239.
[16] C. Boissiere, D. Grosso, A. Chaumonnot, L. Nicole, C. Sanchez, Aerosol route to functional nanostructured inorganic and hybrid porous materials, Adv. Mater., 23 (2011) 599-623.
[17] D.P. Debecker, Innovative sol-gel routes for the bottom-up preparation of heterogeneous catalysts, Chem. Rec., 18 (2018) 662-675.
[18] D.P. Debecker, M. Stoyanova, U. Rodemerck, F. Colbeau-Justin, C. Boissère, A. Chaumonnot, A. Bonduelle, C. Sanchez, Aerosol route to nanostructured WO_3-SiO_2-Al_2O_3 metathesis catalysts: toward higher propene yield, Appl. Catal., A, 470 (2014) 458-466.
[19] N. Godard, A. Vivian, L. Fusaro, L. Cannavicci, C. Aprile, D.P. Debecker, High-yield synthesis of ethyl lactate with mesoporous tin silicate catalysts prepared by an aerosol-assisted sol–gel process, ChemCatChem, 9 (2017) 2211-2218.
[20] V. Smeets, C. Boissière, C. Sanchez, E.M. Gaigneaux, E. Peeters, B.F. Sels, M. Dusselier, D.P. Debecker, Aerosol route to TiO_2–SiO_2 catalysts with tailored pore architecture and high epoxidation activity, Chem. Mater., 31 (2019) 1610-1619.
[21] Z. Guo, G. Xiong, L. Liu, P. Li, L. Hao, Y. Cao, F. Tian, Aerosol-assisted synthesis of hierarchical porous titanosilicate molecular sieve as catalysts for cyclohexene epoxidation, J. Porous Mater., 23 (2016) 407-413.
[22] S. Maksasithorn, P. Praserthdam, K. Suriye, D.P. Debecker, Preparation of super-microporous WO_3–SiO_2 olefin metathesis catalysts by the aerosol-assisted sol–gel process, Microporous Mesoporous Mater., 213 (2015) 125-133.
[23] S. Pega, C. Boissière, D. Grosso, T. Azaïs, A. Chaumonnot, C. Sanchez, Direct aerosol synthesis of large-pore amorphous mesostructured aluminosilicates with superior acid-catalytic properties, Angew. Chem. Int. Ed., 48 (2009) 2784-2787.
[24] A. Vivian, L. Fusaro, D.P. Debecker, C. Aprile, Mesoporous methyl-functionalized Sn-silicates generated by the aerosol process for the sustainable production of ethyl lactate, ACS Sustainable Chem. Eng., 6 (2018) 14095-14103.
[25] C.R. Bayense, A.P.M. Kentgens, J.W. De Haan, L.J.M. Van de Ven, J.H.C. Van Hooff, Determination of gallium in H(Ga)ZSM5 zeolites by gallium-71 MAS NMR spectroscopy, J. Phys. Chem., 96 (1992) 775-782.
[26] M. Chatterjee, T. Iwasaki, Y. Onodera, T. Nagase, H. Hayashi, T. Ebina, Characterization of ordered mesoporous gallium MCM-41 synthesized at room temperature, Chem. Mater., 12 (2000) 1654-1659.
[27] C.-F. Cheng, H. He, W. Zhou, J. Klinowski, J.A.S. Gonçalves, L.F. Gladden, Synthesis and characterization of the gallosilicate mesoporous molecular sieve MCM-41, J. Phys. Chem., 100 (1996) 390-396.
[28] W. Zhang, C.I. Ratcliffe, I.L. Moudrakovski, J.S. Tse, C.-Y. Mou, J.A. Ripmeester, Characterization of the location and interfacial states of gallium in gallium/MCM-41 composites, Microporous Mesoporous Mater., 79 (2005) 195-203.
[29] H.K.C. Timken, E. Oldfield, Solid-state gallium-69 and gallium-71 nuclear magnetic resonance spectroscopic studies of gallium analog zeolites and related systems, JACS, 109 (1987) 7669-7673.
[30] X. Collard, P. Louette, S. Fiorilli, C. Aprile, High surface area zincosilicates as efficient catalysts for the synthesis of ethyl lactate: an in-depth structural investigation, PCCP, 17 (2015) 26756-26765.
[31] J.L. Bourque, M.C. Biesinger, K.M. Baines, Chemical state determination of molecular gallium compounds using XPS, Dalton Trans., 45 (2016) 7678-7696.
[32] C.D. Wagner, A. Joshi, The auger parameter, its utility and advantages: a review, J. Electron. Spectrosc. Relat. Phenom., 47 (1988) 283-313.
[33] R. Gérardy, R. Morodo, J. Estager, P. Luis, D.P. Debecker, J.-C.M. Monbaliu, Sustaining the transition from a petrobased to a biobased chemical industry with flow chemistry, Top. Curr. Chem., 377 (2018) 1.
[34] R.-l. Liu, H.-q. Zhu, Z.-w. Wu, Z.-f. Qin, W.-b. Fan, J.-g. Wang, Aromatization of propane over Ga-modified ZSM-5 catalysts, J. Fuel Chem. Technol., 43 (2015) 961-969.
[35] G. Moretti, Auger parameter and Wagner plot in the characterization of chemical states by X-ray photoelectron spectroscopy: a review, J. Electron. Spectrosc. Relat. Phenom., 95 (1998) 95-144.
[36] G. Moretti, F. Filippone, M. Satta, Use of Auger parameter and Wagner plot in the characterization of Cu‐ZSM‐5 catalysts, Surf. Interface Anal., 31 (2001) 249-254.
[37] C. Wagner, A. Joshi, The auger parameter, its utility and advantages: a review, J. Electron. Spectrosc. Relat. Phenom., 47 (1988) 283-313.
[38] G. Moretti, A. Palma, E. Paparazzo, M. Satta, Auger parameter and Wagner plot studies of small copper clusters, Surf. Sci., 646 (2016) 298-305.
[39] D. Massiot, I. Farnan, N. Gautier, D. Trumeau, A. Trokiner, J.P. Coutures, ^{71}Ga and ^{69}Ga nuclear magnetic resonance study of β-Ga_2O_3: resolution of four- and six-fold coordinated Ga sites in static conditions, Solid State Nucl. Magn. Reson., 4 (1995) 241-248.
[40] B. Bonelli, B. Onida, J.D. Chen, A. Galarneau, F. Di Renzo, F. Fajula, E. Garrone, Spectroscopic characterisation of the strength and stability of the acidic sites of Al-rich microporous micelle-templated silicates, Microporous Mesoporous Mater., 67 (2004) 95-106.
[41] M.R. Nanda, Z. Yuan, W. Qin, H.S. Ghaziaskar, M.-A. Poirier, C.C. Xu, Thermodynamic and kinetic studies of a catalytic process to convert glycerol into solketal as an oxygenated fuel additive, Fuel, 117 (2014) 470-477.
[42] L.A. Bivona, A. Vivian, L. Fusaro, S. Fiorilli, C. Aprile, Design and catalytic applications of 1D tubular nanostructures: Improving efficiency in glycerol conversion, Appl. Catal., B, 247 (2019) 182-190.
[43] A. Vivian, L. Soumoy, L. Fusaro, S. Fiorilli, D.P. Debecker, C. Aprile, Surface-functionalized mesoporous gallosilicate catalysts for the efficient and sustainable upgrading of glycerol to solketal, Green Chem., 23 (2021) 354-366.
[44] H. Hussein, A. Vivian, L. Fusaro, M. Devillers, C. Aprile, Synthesis of highly accessible gallosilicates via impregnation procedure: enhanced catalytic performances in the conversion of glycerol into solketal, ChemCatChem, 12 (2020) 5966-5976.
[45] F. Schüth, M.D. Ward, J.M. Buriak, Common pitfalls of catalysis manuscripts submitted to chemistry of materials, Chem. Mater., 30 (2018) 3599-3600.
[46] K. Stawicka, A.E. Díaz-Álvarez, V. Calvino-Casilda, M. Trejda, M.A. Bañares, M. Ziolek, The role of Brønsted and Lewis acid sites in acetalization of glycerol over modified mesoporous cellular foams, J. Phys. Chem. C, 120 (2016) 16699-16711.
[47] L. Li, T.I. Korányi, B.F. Sels, P.P. Pescarmona, Highly-efficient conversion of glycerol to solketal over heterogeneous Lewis acid catalysts, Green Chem., 14 (2012) 1611-1619.

SUPPORTING INFORMATION

The high activity of mesoporous Ga-SiO_2 catalysts in the upgrading of glycerol to solketal explained by in-depth characterization

Alvise Vivian,[a] Loraine Soumoy,[a] Luca Fusaro,[a] Pierre Louette,[b] Alexandre Felten,[b] Sonia Fiorilli,[c] Damien P. Debecker,[d,*] and Carmela Aprile[a,*]

[a] Unit of Nanomaterials Chemistry (CNANO), Department of Chemistry, University of Namur, 5000 Namur, Belgium
[b] SIAM, Department of Physics, University of Namur, 5000 Namur, Belgium
[c] Department of Applied Science and Technology, Politecnico di Torino, 10129 Torino, Italy
[d] Institute of Condensed Matter and Nanosciences - UCLouvain, 1348 Louvain-la-Neuve, Belgium

Figure S1. N_2 adsorption-desorption isotherms (a) and BJH pore size distribution (b) of pristine SiO_2 and gallium oxide impregnated on pristine silica (Ga_2O_3-SiO_2)

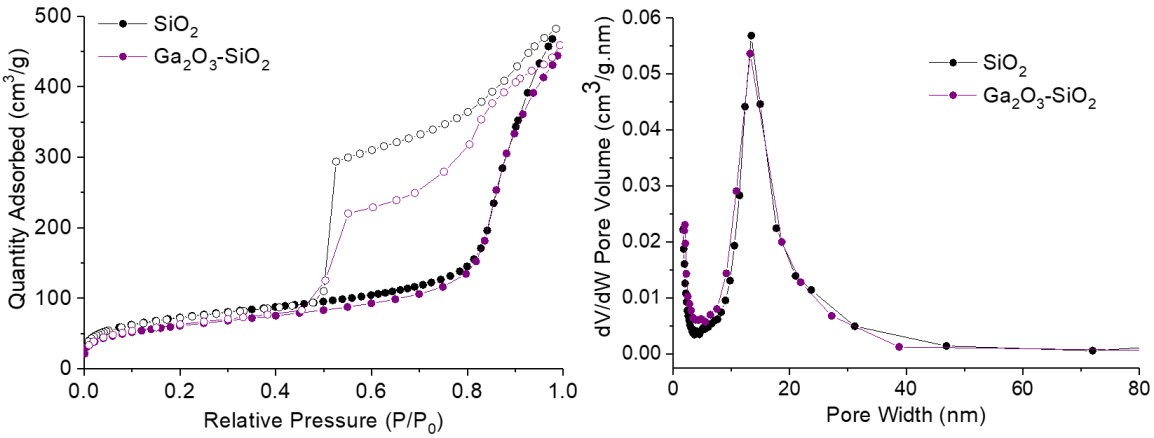

506

507 **Table S1.** Textural properties and composition of pristine SiO_2 and gallium oxide impregnated on pristine
508 silica (Ga_2O_3-SiO_2)

509

Material	Surface Area ($m^2 \cdot g^{-1}$)	BJH pore width (nm)	Pore Volume (cm^3/g)	Si/Ga[a]
SiO_2	230	13.5	0.6	-
Ga_2O_3-SiO_2	210	13.2	0.6	38

[a] determined via ICP-OES analysis

510

511

512 **Figure S2.** Particle size distribution of a) Ga-37, b) Ga-74 and c) Ga-148

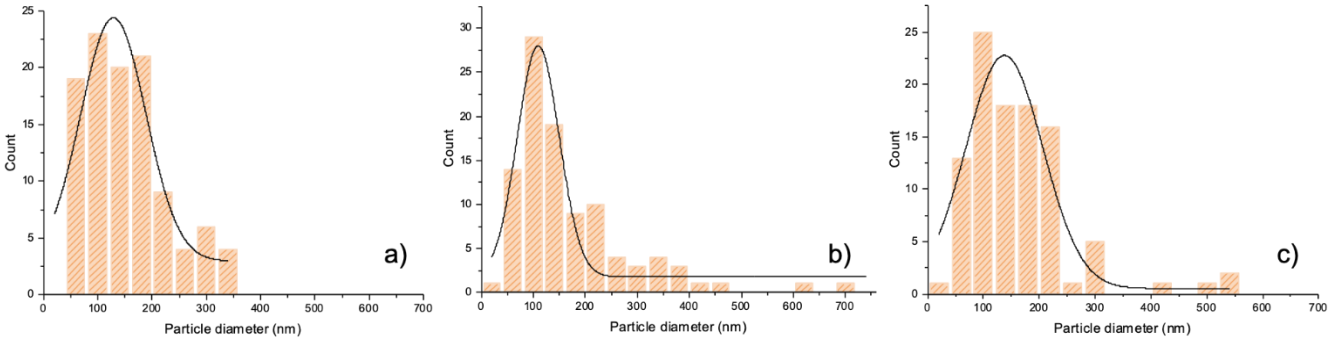

513

514 **Figure S3.** ^{29}Si DE-MAS NMR (direct excitation) of a) Ga-37, b) Ga-74 and c) Ga-148

515

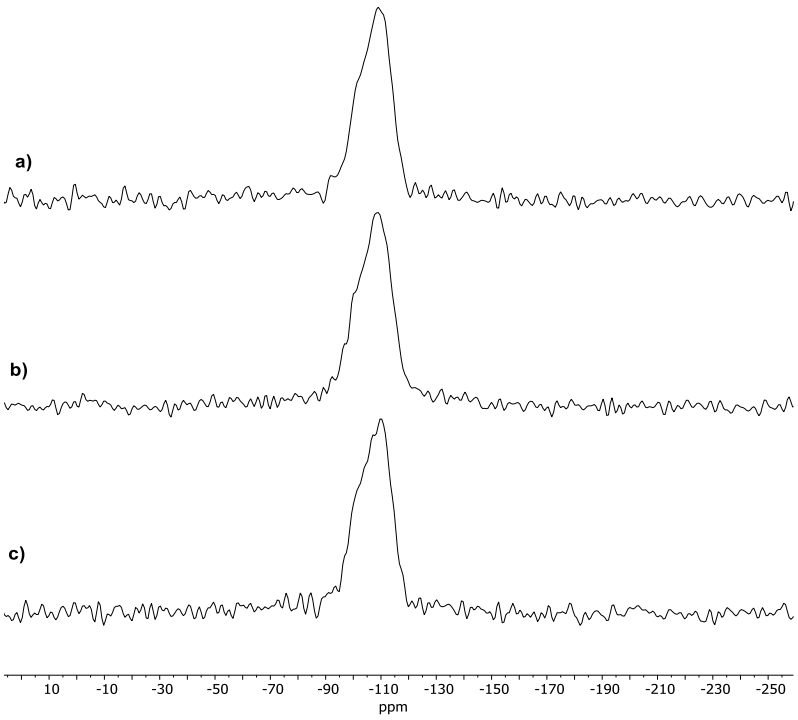

516

517

518 **Figure S4.** XPS analysis of 2p levels on Ga-74, Ga-37 and hydrated Ga_2O_3

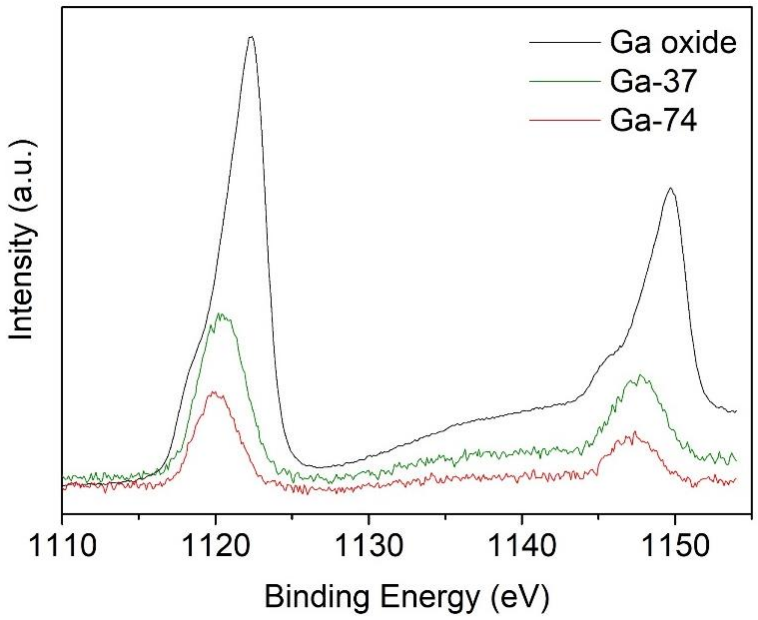

519

520

521 **Figure S5.** ^{71}Ga solid state MAS NMR spectrum of pure β-Ga_2O_3, registered at 12.5 kHz, used as NMR
522 reference compound. The spectrum presents the same pattern of signals, as reported in the literature by
523 [D. Massiot, I. Farnan, N. Gautier, D. Trumeau, A. Trokiner and J. P. Coutures, Solid State Nuclear Magnetic
524 Resonance, 1995, 4, 241-248.]

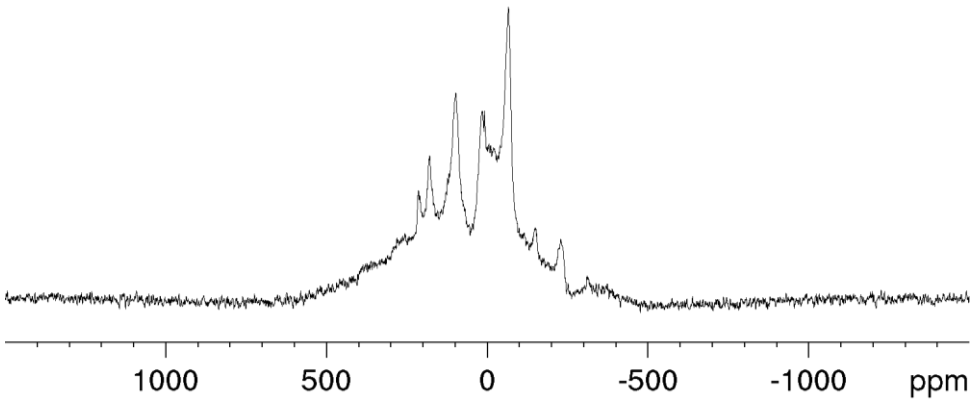

525

526

527 **Figure S6.** Wide angle XRD patterns of Ga-37, Ga-74 and Ga-148

528

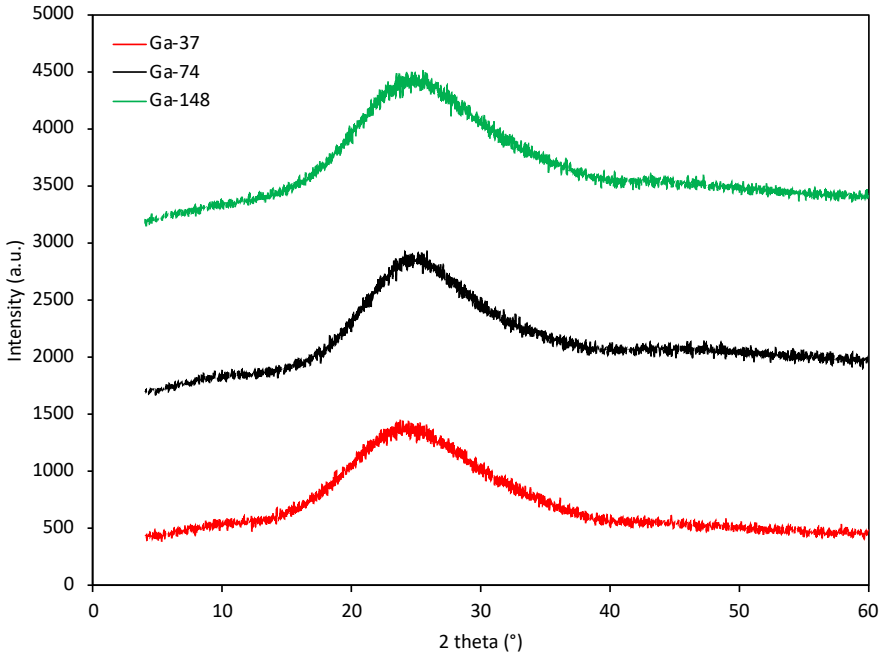

529

530

531

532

533 **Figure S7.** FT-IR spectra of Ga-37 (red curve), Ga-74 (blue curve) and Ga-148 (green curve) after outgassing
534 of ammonia at RT

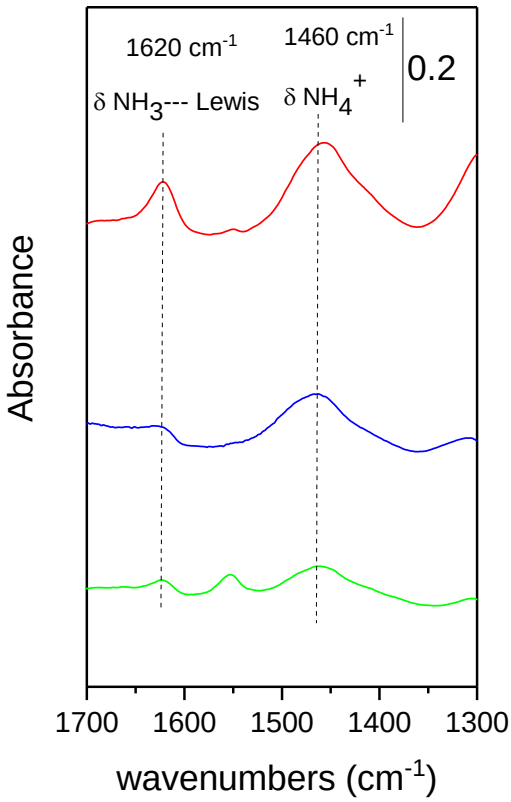

Figure S8. NH_3-TPD of Ga-37 and Ga-74 catalysts (left) and quantification of the acid sites (right). The total amount of acidic sites is determined by integrating the area under the TPD profile, after calibrating the apparatus with a diluted feed of ammonia of known composition.

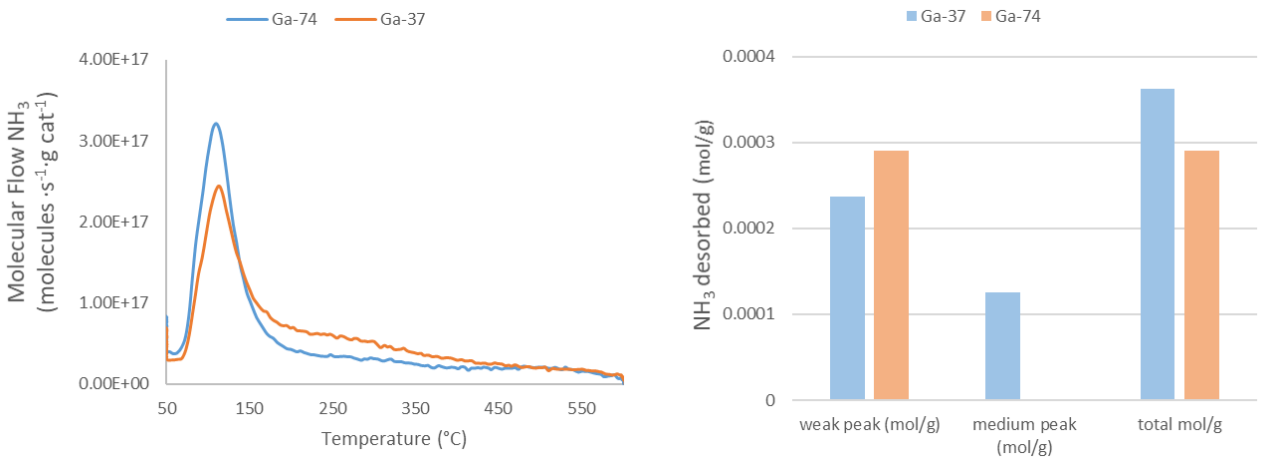

Figure S9. Proposed mechanism for the acetalization of glycerol catalyzed by (a) Brønsted acid site or (b) Lewis acid site

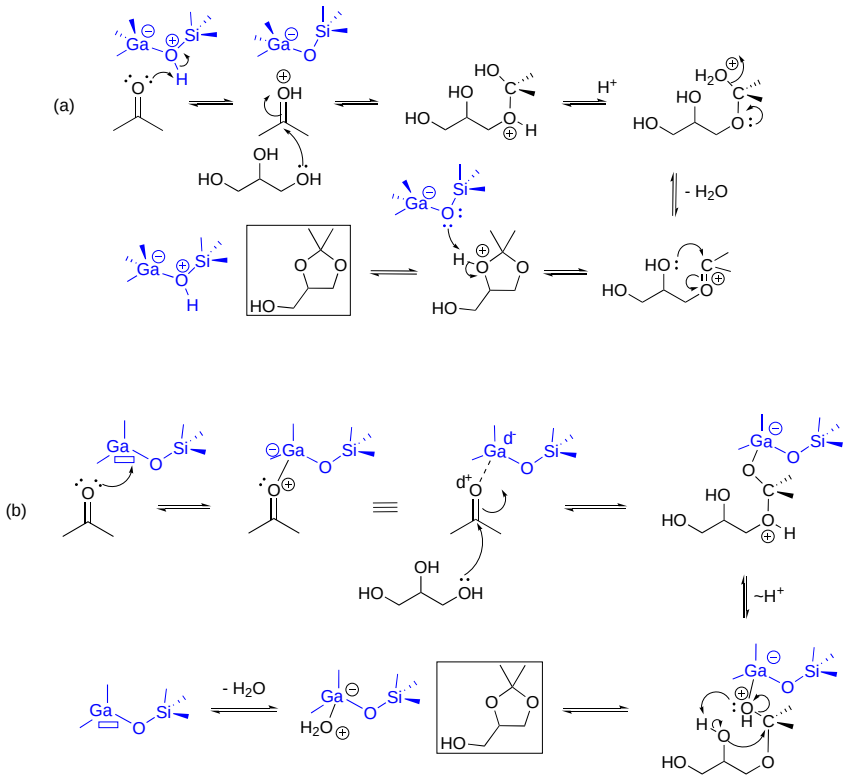

Table S2. Detailed catalytic results of Ga-74 and reference catalysts. Reaction conditions: 0.01 mol of glycerol, 1 eq of acetone, 0.02 mol of t-butanol, 25 mg of catalyst, 80°C

Solid	Reaction time (h)	Yield (%)	Si/M	TOF
Ga-74	2	30	79	290
Al-TUD-1	6	28	50	61
Zr-TUD-1	6	46	51	127
Sn-MCM-41	6	42	54	102
XS-Ga-MCM-41	6	25	44	60

Figure S10. ^{71}Ga solid state MAS NMR spectra of fresh Ga-74 catalyst (a) and used Ga-74 after the 4th catalytic cycle (b)

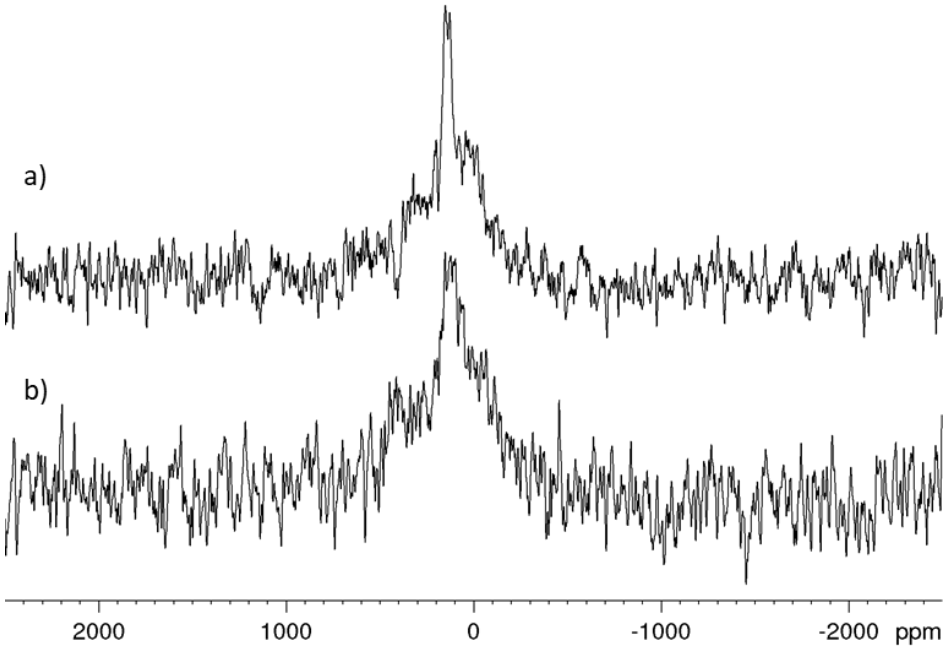

Table S3. Textural properties and composition of Ga-74 catalyst after the 4th catalytic cycle

Material	Surface Area ($m^2 \cdot g^{-1}$)	BJH pore width (nm)	Si/Ga[a]
Ga-74 fresh	350	7.0	79
Ga-74 4th cycle	335	6.8	76

[a]determined via ICP-OES analysis

Figure S11. Hot filtration test with Ga-74. Reaction conditions: 25mg of catalyst, glycerol (0.92 g, 0.01 mol), absolute EtOH (0.70 mL) acetone (2.32 g, 4 equiv.). After 1 h, the catalyst was separated from the reaction mixture by hot filtration (~ 50 °C) (see experimental part).

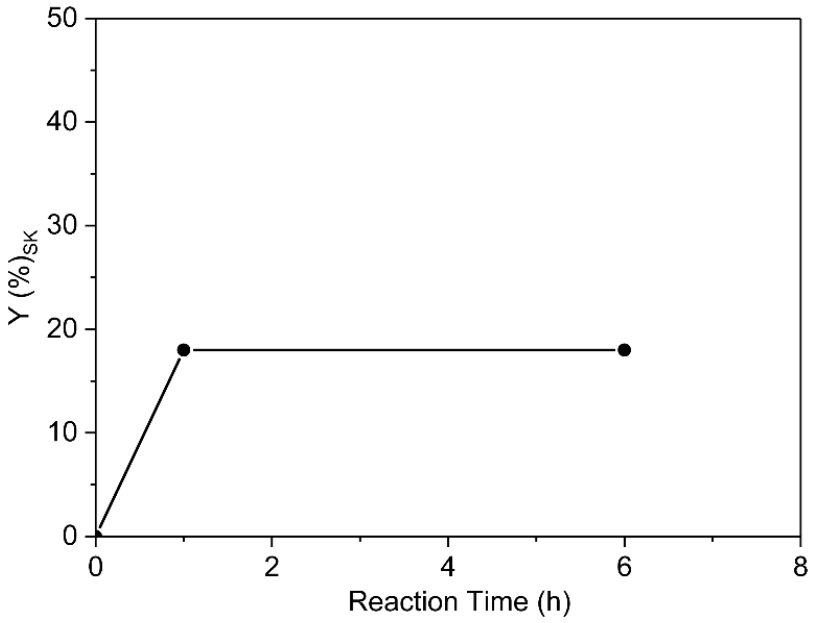

570

571

572